DALHOUSIE UNIVERSITY

Static and Dynamic Characteristics of Nano-Reinforced 3D-Fiber Metal Laminates Using Non-Destructive Techniques

B. Soltannia[1], P. Mertiny[1] and F. Taheri[2,*]
[1]Department of Mechanical Engineering, University of Alberta, Donadeo Innovation Centre for Engineering, 9211-116 Street NW, Edmonton, Alberta, T6G 1H9, Canada
[2,*]Department of Mechanical Engineering, Dalhousie University, 1360 Barrington Street, PO Box 15000, Halifax, NS, B3H 4R2, Canada
[*]Corresponding author: (farid.taheri@dal.ca)

Abstract

Uncontrolled vibration in mechanical systems (e.g. aircraft, trains and automobiles) may result in undesirable noise and eventually, cause mechanical failure. In this context, the main objective of the present research is to explore parameters that govern and affect the frequency response of three-dimensional fiber metal laminates (3DFMLs). 3DFMLs are a class of novel lightweight hybrid material systems with great potential for use in aforementioned applications. Therefore, the vibration characteristics of the two most commonly used configurations of 3DFMLs are experimentally investigated by nontraditional and conventional approaches. The material damping is also improved by the inclusion of two different types of nanocarbon particles (NCP) within the core and/or interfaces of the hybrid system. The results are presented and compared. The inclusion of NCP improved the fundamental frequency of the system slightly; however, material damping was enhanced significantly when only 1 wt% NCP was used in the interfacial sections of the system.

Keywords: Fiber-metal Laminates, Vibration, Damping, Non-destructive Testing, Carbon Nanoparticles.

1 Introduction

Fiber-reinforced polymer (FRP) composites offer superior specific strength, stiffness and durability compared to most metallic materials [1,2]. FRPs are corrosion resistant and highly tailorable materials. They also possess high energy absorption capacity and controllable damage mechanism [3–5]. These characteristics make them highly effective and desirable compared to many materials traditionally used in various applications [6–11]. As a result, FRPs are increasingly employed in primary and non-primary structural applications in the aerospace, infrastructure, marine, automotive, offshore/onshore oil and gas industries. Amongst the positive attributes of FRP composites is their favorable vibration damping capacity, which outperforms most other materials. This characteristic is an important feature of this class of materials, since excessive and unharnessed vibration in structures may result in undesirable consequences, such as unwanted noise and even failure of the structure. Such problems are often encountered in transport vehicle body components, airplane cabins, and train and subway enclosures.

Spanning several decades, vibration analyses of composite materials and structures (thin and thick laminates and sandwich configurations) have been the focus of multiple analytical, numerical and experimental studies [12]. In 1973, Noor [13] pointed out the inadequacies of available analytical models for evaluating the low-frequency response of simply-supported thick composite beams. Since then, several researchers have employed and modified the classical Rayleigh-Ritz method, which has often been used to evaluate the natural frequencies of thin or thick laminates and sandwich plates [14–16]. For instance, Hu et al. [17] analyzed the vibration response of twisted angle-ply laminated plates using the Rayleigh-Ritz method based on the Mindlin plate theory. In another work, Lei et al. [18] utilized the Ritz method to investigate the damping properties of functionally graded thin laminate composite plates, reinforced with carbon nanotubes (CNT), with clamped boundary conditions. Chen et al. [19] used Galerkin's method to analyze the nonlinear vibration response of rectangular laminated composite plates. Kant and Swaminathan [20] developed a higher-order theory, considering through-thickness shear effects for analyzing the free vibration of sandwich plates. Tu et al. [21] formulated a finite element approach to model the vibration and bending characteristics of laminated and sandwich composite plates using a nine-node rectangular element formulated based on a higher-order shear-deformation theory, thereby accounting for the variation of the through-the-thickness shear.

Improving the damping characteristics of laminated or sandwich composite plates has also been explored experimentally by several researchers. The use of inherently damped materials and nanoparticles (NPs) as passive damping tools on the one hand, and the use of external damping sources as an active damping strategy on the other hand, have been found to generate the most effective approach for enhancing the dynamic damping properties of composite materials and structures. Zou et al. [22], Hajikhani et al. [23], Soltannia et al. [24,25], and De Cicco and Taheri [26] experimentally investigated the vibration characteristics of laminated and sandwich composite beams using nondestructive testing (NDT) techniques. Similarly, Cheraghi et al. [27] used the impulse excitation technique along with the use of piezoelectric sensors to establish the damping response of polyvinyl chloride (PVC) pipes. The accuracy of various methods for retrieving the damping coefficient from the acquired vibration data has also been explored by a few researchers [22,28,29].

Various approaches have also been explored to improve the material damping response. A notable example would be the approach adopted by Berthelot [6,30], Piollet et al. [31], and Fotsing et al. [32,33], who investigated the effect of entangled cross-linked fibers and interleaved viscoelastic layers (as inherently damped materials) in damping the vibration response of laminate and sandwich composites. Sargianis et al. [34] demonstrated the use of naturally damped materials to augment the structural damping ratio of sandwich composite plates by 100%. They used balsa wood for the core and natural fibers to form the facial laminate constituents of their sandwich plates. They also incorporated a synthetic core material (Rohacell®51 WF) instead of the balsa core, achieving an impressive damping enhancement of 233% at the expense of a marginal loss of flexural bending rigidity (FBR).

The advantages of including small amounts of NPs to improve the mechanical and electrical properties of the matrix of laminated polymer composite structures and adhesives have been actively investigated by several researchers in recent years [35–42]. Ahmadi-Moghadam et al. [43] demonstrated that the use of chemically functionalized graphene nanoplatelets (GNP) can result in much greater improvement in the mechanical and fracture response of composite materials compared to non-functionalized GNP. Liu et al. [44] investigated the effect of functionalized single-wall carbon nanotubes (SWCNT) on the damping properties of composite materials.

DeValve and Pitchumani [45] experimentally investigated the effect of adding CNT on damping enhancement of carbon fiber reinforced polymer (CFRP) laminated composite beams. The addition of merely 1 to 2 wt% CNT improved the damping properties by 40 to 60%. Similarly, Khan et al. [46] showed that the inclusion of multi-wall carbon nanotubes (MWCNT) enhanced the damping properties of cantilever CFRP beams. They highlighted that the improved damping performance of their beams was a result of enhanced beam stiffness facilitated by the MWCNT.

To establish the improvement gained in mechanical properties of composites by various approaches as briefly described above, many investigators have used traditional techniques such as those developed by the National Aeronautics and Space Administration (NASA) [47], or those described in various ASTM Standards [48,49]. In addition, several novel and mainly nondestructive approaches have also been developed by researchers. For instances, Viens and Johnson [28] discussed the effectiveness of using the dynamic excitation technique for evaluating the elastic properties of composites non-destructively. They demonstrated the utility of GrindoSonic devices [50] as an effective tool for evaluating the elastic properties of composite beams nondestructively and with acceptable accuracy.

At this juncture, and beside many other techniques to enhance stiffness-to-weight ratio by introducing high performance pseudo-ductile (HiPerDuCT) composites utilizing only FRP composite materials [51], it is worth mentioning some of the relatively recent efforts expended in developing more resilient, cost-effective and lightweight hybrid materials, notably, fiber-metal laminates (FMLs) [52,53]. FMLs are hybrid laminates consisting of thin alternating bonded layers of thin metallic sheets (e.g., aluminum or magnesium alloys) and fiber/epoxy [54]. FMLs were developed first in the early 1980s as a more cost-effective alternative to CFRP used in the aerospace industry. The first FML was ARALL (an acronym for aramid reinforced aluminum laminate), developed by Delf Student, Marissen, which consists of a layout of aramid fiber layers with aluminum layers [55]. Since these pioneering efforts, various FMLs have been developed and produced using different fiber types, such as carbon and aramid. A new rendition of conventional thin FMLs was recently introduced by Asaee and Taheri [56], thereafter referred to as three-dimensional FLM (3DFML). This class of FML has been demonstrated to possess exemplary characteristics compared to conventional FRPs and FMLs, especially from the perspective of

crashworthiness and impact tolerance, as demonstrated in [57]. A 3DFML is essentially a sandwich composite consisting of a novel 3D fiberglass fabric (3DFGF), sandwiched between thin sheets of a lightweight metallic alloy (e.g., aluminum or magnesium alloys). The superior responses of various configurations of this class of 3DFML under static and dynamic loading conditions have been demonstrated, promising the suitability of this type of FML in forming lightweight structural panels, especially for meeting recent weight reduction and thus fuel efficiency targets in the automotive industry [24–26,56], beside many other techniques to enhance stiffness-to-weight ratio by introducing high performance pseudo-ductile (HiPerDuCT) composites utilizing only FRP composite materials [51].

2 Research Objectives of this Study

Several investigations revealed the superior mechanical response of 3DFMLs to lateral and axial loading at various rates, see e.g. [56,57]. However, only a preliminary investigation has been conducted to assess the vibration characteristics of this interesting material class [24–26]. The latter study speculated that one could further improve the vibration response of 3DFMLs by inclusion of suitable NPs. Therefore, the objectives of the present study are twofold. First, to investigate the different parameters that affect and govern the vibration response of 3DFMLs. Under this objective, the 3DFML configuration that would possess the highest damping and optimal noise and vibration reduction attributes shall be identified. Secondly, the potential of enhancing the vibration characteristics of 3DFMLs by incorporating NPs within the hybrid system shall also be explored. In this regard, an attempt was made to improve the material damping characteristics by including NPs within the core and/or interface layers of the hybrid system to establish the 3DFML configuration that would generate the most effective damping response. For that, two types of nanocarbon particles (NCP), namely MWCNT and functionalized GNP were employed, thereby establishing an effective nanocomposite for enhancing the vibration response of 3DFMLs. The results obtained by various NDT characterization approaches are presented, and recently developed methods are contrasted with a traditional technique in order to verify the accuracy of novel NDT methods and equipment. Figure 1 shows a graphical illustration of the topics considered in the present experimental investigation that are described in detail in the remaining parts of this paper.

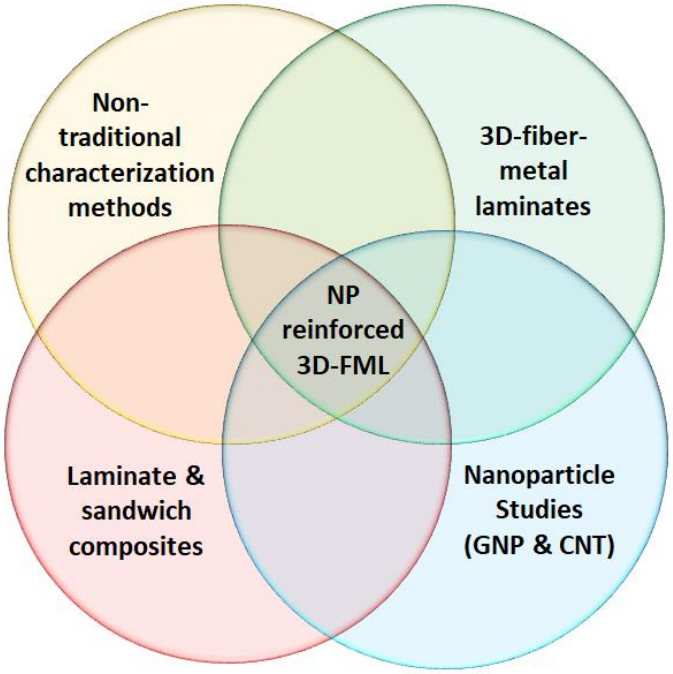

Figure 1. Schematic of research subjects considered in the present work.

3 Materials and Fabrication

3.1 Materials

3DFGF was procured from China Beihai Fiberglass Co. (Jiujiang City, Jiangxi, China). For 3DFMLs with metal face sheets, magnesium alloy sheets (type AZ31B-H24) with thickness of 0.5 mm were purchased from MetalMart International (Commerce, CA, USA). A hot-cure epoxy resin was used for fabricating the 3DFGF constituents. This two-part resin system was composed of bisphenol-A based Araldite LY 1564 resin and Aradur 2954 cycloaliphatic polyamine hardener (Huntsman Co., West Point, GA, USA). For bonding magnesium face sheets to 3DFGF cores, a two-part cold-cure epoxy resin was applied at the interface (105 resin and 206 hardener, West System, Bay City, MI, USA). To facilitate certain material characterization tasks an alternative core material was employed, which was a two-part urethane foam with free rise density of 128 kg/m^3 (8 lb/ft^3) supplied by US Composites (West Palm Beach, FL, USA). To serve as a baseline for comparison with various composite sandwich configurations, as well as for the fabrication of some samples, an aluminum (Al) plate material (type 6061-T6) with thickness of 4 mm was obtained from a local supplier.

Two types of NCP were chosen to be dispersed within the epoxy resins. They were (i) functionalized GNP (type GNP-M-25) with an average diameter of 25 μm, thickness of 6 nm, and surface area of 100 m^2/g (XG Science Ltd., Lansing, MI, USA); and (ii) MWCNT with purity greater than 95% and outer diameters ranging between 5 and 15 nm (US Research Nanomaterials, Inc., Houston, TX, USA).

3.2 Specimen Manufacturing

3.2.1 3DFGF Specimens

3DFGF was utilized in two forms: (i) 3DFGF was used to generate monolithic 3DFGF sandwich plates; and (ii) 3DFGF formed the core region of the magnesium alloy faced 3DFML panels investigated in this study. In either case, to create panels, the hot-cure epoxy resin was brushed onto the fabric. It should be mentioned that the 3DFGF, which in its dry state is flat, 'awakens' upon resin impregnation, creating several rows of identical sized channels (or cavities) within the thickness of the fabric. Each resin-impregnated fabric was then cured in an oven at 60°C for 2 hours and then at 120°C for 8 hours. After curing, at least three beam specimens were cut from each panel. 3DFGF specimen dimensions were 200 mm by 20 mm by 4 mm, referring to the beam length, *L*, width, *b*, and thickness, *h*, respectively, the same as for all other specimens unless specified otherwise (e.g., in case of foam core sandwich beams). Preform 3DFGF specifications have been listed in table 1 [58].

Table 1. Preform 3DFGF specifications [58].

Area Weight (g/m^2)	Core Thickness (mm)	Density of Warp (ends/cm)	Density of Weft (ends/cm)	Tensile strength Warp (n/50mm)	Tensile strength Weft (n/50mm)
740	2	18	12	4500	7600
800	4	18	10	4800	8400
1480	10	15	8	6800	12000

Also, picture of preform 3DFGF and its resin impregnated composite, as well as 3DFGF with different thicknesses have been shown in Figure 2 [58].

(a) (b) (c)

Figure 2. 3DFGF images: (a) preform 3DFGF; (b) its resin impregnated composite; and (c) 3DFGF with different thicknesses. [58]

3.2.2 3DFML Specimens

To form the 3DFML panels, the processed 3DFGF panels were sandwiched between a pair of magnesium sheets. The sheets were initially roughened by grit-blasting and cleaned with an air gun, followed by acetone washing and air-drying. They were then bonded to the 3DFGF core using the cold-cure epoxy resin. Resulting sandwich panels were cured for at least 24 hours at room temperature under vacuum to ensure high-quality interface-bonding. Additional details on the fabrication procedure of the 3DFMLs can be found in [56].

3.2.3 Foam Core Sandwich Specimens

In order to establish the elastic modulus of the main 3DFGF constituents (i.e., the biaxial fabrics forming the two outer panels of the 3DFGF), a series of sandwich specimens were fabricated in conformance with the ASTM D7249 standard [59]. For that, first, the foam core section of the sandwich panel was fabricated by pouring the two-part urethane foam (1:1 mix) in between the space created between two clamped aluminum plates, separated by 4 mm spacers. The foam-mating surfaces of the plates were covered with non-porous Teflon sheets. The foam was let to cure at room temperature for 24 hours. Subsequently, two pieces of 3DFGF fabrics were resin impregnated (using the hot-cure epoxy system) and then placed in an oven for curing while applying vacuum bagging so that the 3DFGF fabrics would remain in their 2D state. Then, the foam panel was sandwiched in between the two fabrics, using the cold-cure resin system for

bonding. The resulting assembly was cured at room temperature under vacuum, yielding the final sandwich configuration required for testing. Appropriately sized specimens fabricated in conformance with the ASTM D7249 standard [59] having length, width and total thickness of 275 mm, 20 mm and 8.5 mm, respectively, were extracted from the fabricated foam core sandwich plates to establish the elastic modulus of the biaxial fabrics forming the two outer panels of the 3DFGF. Specimens were cut using a diamond blade saw.

3.2.4 NCP Reinforced 3DFGF and 3DFML Specimens

In order to create NCP reinforced 3DFGF and 3DFML specimens, NCP modified resin was first prepared as follows. For each type of NCP, filler particles with 1 wt% (by weight concentration) were dispersed in the resin system using a mechanical stirrer set at a speed of 2000 rpm for 10 minutes. Then, the NCP resin slurry was calendered using a three-roll mill homogenizer (Torrey Hills Technologies, San Diego, CA, USA). The roller gaps were set at 30 μm using a feeler gauge. In this study, the roller speed was set at a constant rate of 174 rpm. To maximize the quality of dispersion, calendering was conducted seven times. The curing agent was subsequently blended with the resin slurry using the stirrer at a speed of 400 rpm for 4 to 6 minutes. The mixture was then degassed under 711 Torr (28” Hg) vacuum for 2 to 3 minutes. The interested reader is referred to [38,43] for information on NCP functionalization and particle dispersion and calendaring processes.

To study the morphology of NCP modified 3DFGF-epoxy panels, a jeweler saw was used to extract samples from several panel locations for field emission scanning electron microscopy (FESEM) using a S-4700 device by Hitachi High-Technologies (Tokyo, Japan). Samples for microscopic analysis were palladium-gold coated using a sputtering device (Model ACE200, Leica, Wetzlar, Germany).

3.2.5 Specimen Configurations and Nomenclature

Various specimen types were fabricated as per the procedures described in the preceding sections. The different specimen configurations are listed in Table 2 along with the abbreviations used to identify samples throughout this study. In the remainder of this document, data is also presented

using an abridged nomenclature to ease the identification of specimens or groups thereof, in addition to the specimen identifiers (ID) listed in Table 2. For example, MWCNT-4-3DFML refers to 3DFML specimens having 4 mm thickness and being reinforced with MWCNT. The length and width of all beam specimens reported in this table are 200 mm by 20 mm, respectively.

Table 2. Specimen configurations and nomenclature.

ID	Material	Core thickness	Resin modification	Filler/resin in core	Filler/resin at interface
Al	Al 6061-T6	4 mm			
3DFML1	3DFML	4 mm	Neat	0 wt%	0 wt%
3DFML2	3DFML	4 mm	GNP	0 wt%	1 wt%
3DFML3	3DFML	4 mm	GNP	1 wt%	0 wt%
3DFML4	3DFML	4 mm	GNP	1 wt%	1 wt%
3DFML6	3DFML	4 mm	MWCNT	0 wt%	1 wt%
3DFML7	3DFML	4 mm	MWCNT	1 wt%	0 wt%
3DFML8	3DFML	4 mm	MWCNT	1 wt%	1 wt%
3DFML9	3DFML	10 mm	Neat	0 wt%	0 wt%
3DFML10	3DFML	10 mm	GNP	0 wt%	1 wt%
3DFML11	3DFML	10 mm	GNP	1 wt%	0 wt%
3DFML12	3DFML	10 mm	GNP	1 wt%	1 wt%
3DFML14	3DFML	10 mm	MWCNT	0 wt%	1 wt%
3DFML15	3DFML	10 mm	MWCNT	1 wt%	0 wt%
3DFML16	3DFML	10 mm	MWCNT	1 wt%	1 wt%
3DFGF17	3DFGF	4 mm	Neat	0 wt%	
3DFGF18	3DFGF	4 mm	GNP	1 wt%	
3DFGF19	3DFGF	4 mm	MWCNT	1 wt%	
3DFGF20	3DFGF	10 mm	Neat	0 wt%	
3DFGF21	3DFGF	10 mm	GNP	1 wt%	
3DFGF22	3DFGF	10 mm	MWCNT	1 wt%	

4 Experimentation

4.1 Vibration Testing

The instrumentation used to acquire vibration signals employed contact type and non-contact type techniques. As illustrated in Figure 3, the contact type device was a GrindoSonic instrument (GS) model MK5i (Leuven, Belgium). The non-contact type device was a laser-Doppler vibrometer (LDV) (Model LP01, Optical Measurement System, Laguna Hills, CA, USA). Also shown in Figure 3 are two prismatic low-density foam sponges supporting a specimen during testing. This

setup mimics a free-free boundary condition. A light-weight hammer, consisting of a steel ball attached to a thin wooden rod, was used to excite the specimens, as per the GS technical documentation [50] and NASA Technical Memorandum 104629 [28].

The prismatic sponge supports were located to coincide with specimens' fundamental vibration mode nodal points. The GS instrument has a small and highly sensitive probe tip (see Figure 3), which was positioned in light contact with the specimens, close to one of the free vibration nodal points, where the vibration amplitude vanishes. The span between nodal points (s), which are distanced equally from each specimen extremity, can be calculated using Eq.(1) [50,60].

$$s = 0.224\, L \tag{1}$$

where L is the beam length. A distance of 45 mm between a support and the corresponding specimen extremity was adjusted for all specimens. The correctness of this distance was confirmed by an eigenvalue finite element analysis conducted earlier by this research group [26,57].

Several researchers demonstrated that data with satisfactory accuracy can be obtained via GS measurements [22,28,29]. However, as mentioned in NASA Technical Memorandum 104629 [28], GS may produce inaccurate results in environments with significant external noise. Inaccurate results are also obtained when a specimen is excited such that higher vibration modes, as opposed to the fundamental mode, are imposed. To mitigate these anomalies, present experiments were conducted in a quiet room. Moreover, all specimens were excited by tapping them at a consistent location (i.e., at a point between the two supports, close to the center span of each specimen).

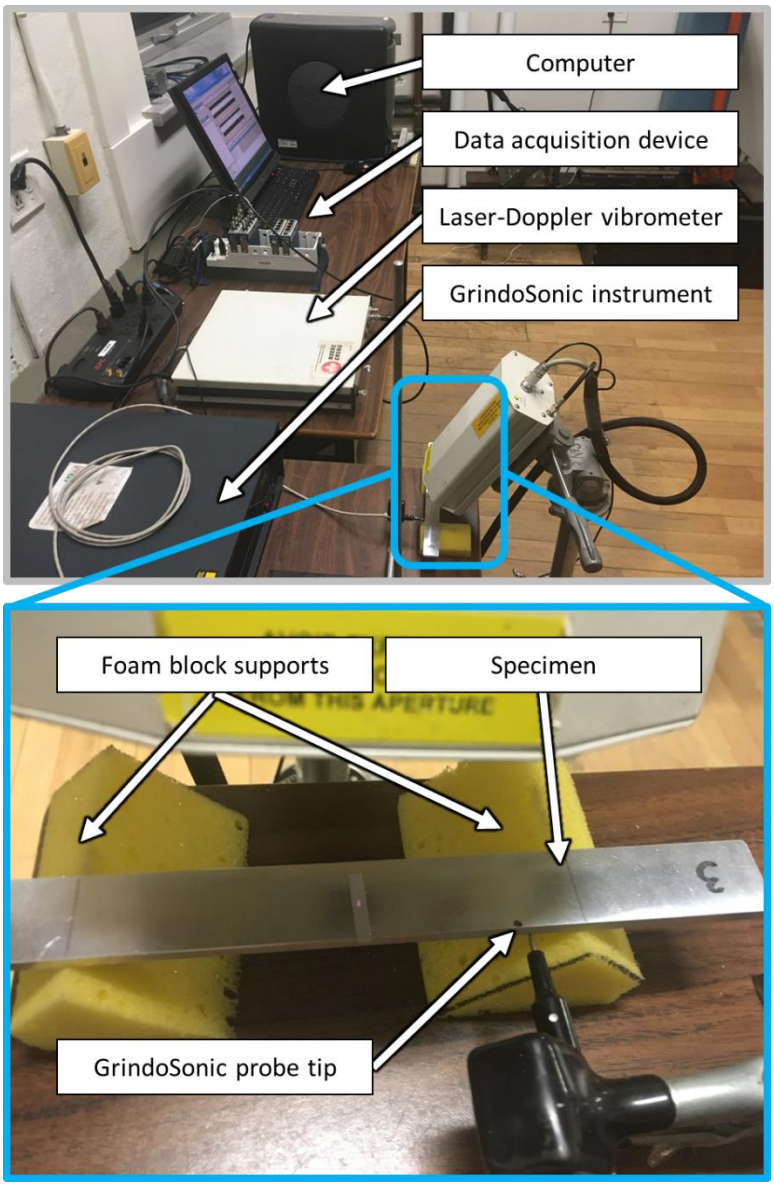

Figure 3. Experimental test setup for recording vibration signals of free-free supported specimens using the GS and LDV.

The outputs from GS and LDV are in the form of an electric potential (voltage), proportional to the amplitude of the excitation. After specimen excitation, the software embedded in the GS automatically analyzes the specimen's oscillatory motion transient response and calculates and displays the specimen's fundamental frequency. However, in order to determine the material damping ratio, the entire oscillation spectrum needs to be captured. Therefore, the GS device was connected to a data-acquisition system (cDAQ-9172, National Instrument, Austin, TX, USA) and a personal computer (PC) running the Signal Express software (2010, National Instruments,

Austin, TX, USA) to record the entire oscillatory spectrum at a 100 kHz sampling rate. The recorded data was then post-processed using the LabVIEW software (2010, National Instruments). For the LDV a laser reflective tape was applied to the specimen to increase the reflected signal intensity.

4.2 Bending Rigidity Testing

The FBR of the various specimens was evaluated employing four-point bending tests according to the pertinent ASTM standard [59]. A servo-hydraulic testing machine equipped with a digital electronic controller was employed for this purpose (2518-610, MTS, Eden Prairie, MN, USA). Figure 4 illustrates the experimental setup. The mid-span deflection of the test specimens was acquired using a laser extensometer (LE-05, Electronic Instrument Research, Irwin, PA, USA). Experimental data in terms of load and deflection was recorded using a PC.

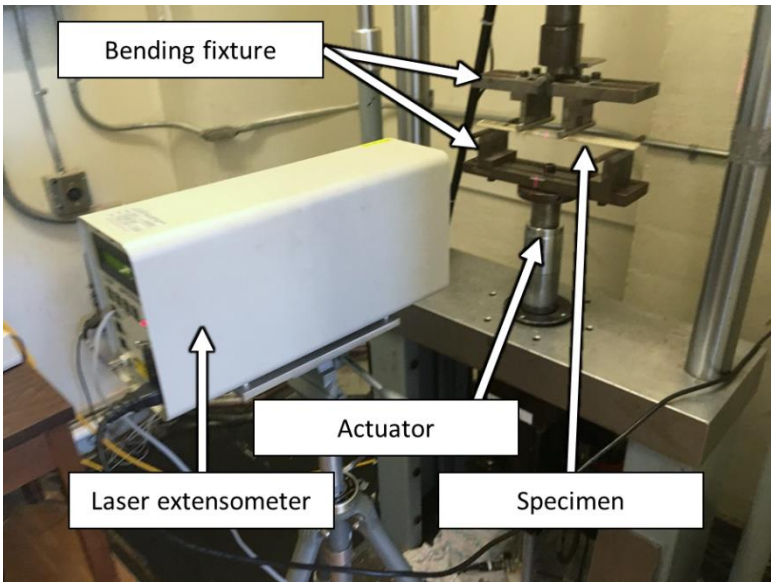

Figure 4. Four-point bending rigidity test setup.

5 Data Analyses

5.1 Fundamental Frequency

The frequencies acquired experimentally using the GS and LDV were contrasted with results from the available closed-form solution given by Eq.(2). The latter was explained extensively in various sources [6,24–26,30,60,61].

$$f_n = \frac{1}{2\pi}\left(\frac{\gamma_n}{L}\right)^2 \sqrt{\frac{R}{\mu}} \quad \text{with} \quad R = \begin{cases} EI & \text{for homogeneous beams} \\ bD_{11} & \text{for composite beams} \end{cases} \tag{2}$$

where f_n is the frequency of the n^{th} vibration mode; γ_n is the n^{th} solution according to Eq.(3) [60]; In this equation, R is the bending rigidity of the beam, and its value, EI, for an isotropic (homogeneous) beam, is replaced by bD_{11} for orthotropic (composite) beam based on homogenization model of material (rule of thumb), where b is the width of the beam, and D_{11} is the bending rigidity per unit width of the laminate in the longitudinal direction, which was obtained experimentally and also calculated analytically, using Eq.(4); μ is the mass per unit length; E is the modulus of elasticity; I is the cross-section moment of inertia about the bending axis.

$$cos\,\gamma\, cosh\,\gamma = 1 \tag{3}$$

Equation (3) is obtained by solving the constitutive equation of motion of a free-free prismatic beam using the separation of variable technique. Since in this study the fundamental bending frequency of the beam is of interest, only the first value for γ_n was computed numerically, yielding $\gamma_1 = 4.73$. Moreover, D_{11} obtained from the experimental data (i.e., load-deflection curves) was contrasted with the analytical solution calculated using Eq.(4) [6–11].

$$D_{11} = \frac{1}{3}\sum_{k=1}^{n} Q_{11}^{k}\,(Z_k^3 - Z_{k-1}^3) \tag{4}$$

where Q is the transformed stiffness matrix of each ply (layer) of the composite material; Z_k and Z_{k-1} refer to the distances measured from the mid-plane of the 3DFGF or 3DFML panels to the bottom and top of each plies (layers), respectively, and k and n indicate correspondingly the individual ply (layer) index and total number of plies in the panel.

5.2 Damping Ratio

Knowledge of a material's damping properties is vital for controlling the vibration response of a given structure that is subjected to vibratory loading. By knowing the damping ratio and natural frequencies, one can simplify a complex vibration analysis into a much simpler equivalent quasi-static analysis. However, conventional techniques used to evaluate the material damping coefficient are very time-consuming, as discussed by Naghipour et al. [62], who used various

characterization techniques to identify the damping coefficient of fiber-reinforced glue-laminated timber beams.

The evaluation of the damping coefficient involves solving the governing constitutive equation of the damped oscillatory motion of a system, represented by Eq.(5) [6,24–26,60]:

$$x_{(t)} = Ae^{-\xi\omega_0 t}\, cos(\omega_{\mathrm{D}} t - \phi) \tag{5}$$

where $x_{(t)}$ is the time (t) dependent motion of a single degree of freedom vibrating mass; A *is* the amplitude; ξ is the damping ratio ($\xi < \xi_c = 1$), with ξ_c being the critical damping ratio; ϕ, ω_0 and ω_{D} are the phase angle, undamped and damped angular natural frequency, respectively. ω_0 and ω_{D} are related to each other according to Eq.(6).

$$\omega_{\mathrm{D}} = \omega_0\sqrt{1-\xi^2} \tag{6}$$

It should be noted that in a damped vibrating system where $\xi < \xi_c = 1$, the amplitude of motion is bound between two exponential curves that form the so-called 'signal envelope'. The half-symmetry envelope of typical signals is illustrated in Figure 5.

The damping coefficient, ξ, can be determined using the logarithmic decrement, δ, of the signal over an oscillation period, T_{D}, using Eq.(7).

$$\xi = \frac{\delta_i}{\sqrt{4\pi^2+\delta_i^2}} \tag{7}$$

where δ_i is the natural logarithm of the ratio of the amplitudes of two successive oscillations. To improve accuracy, the damping ratio can be evaluated over multiple oscillation periods instead of over only one period. The logarithmic decrement and damping coefficient were computed using LabVIEW, employing exponential curve fitting and extraction of curve parameters (power and coefficients).

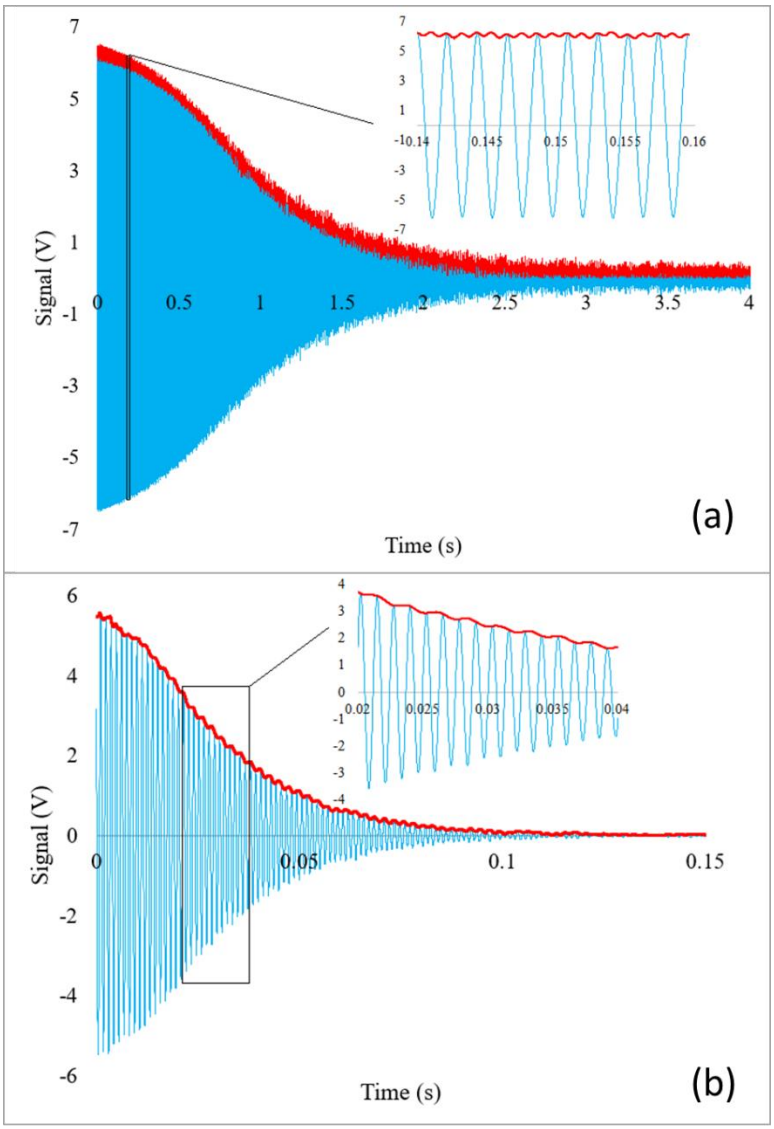

Figure 5. Typical vibration signals and the representative signal envelopes for (a) aluminum and (b) 1% GNP-reinforced 3DFML specimens (GNP in both core and interface).

5.3 Vibration Signal Extraction and Analysis

As mentioned earlier, GS and LDV were used to obtain the fundamental frequency of the beam. The software associated with each instrument calculates the fundamental frequency by measuring the time elapsed between two peak amplitudes of a decaying vibration signal. The results from the instruments were compared against the values obtained from the power spectrum of the entire signal using the 'Spectral Measurements' subroutine of LabVIEW, which is based on the aforementioned analytical equations. In other words, the subroutine takes the vibration signal from

GS and LDV, and yields the amplitude of each frequency of the signal spectrum by employing the Fast Fourier Transform algorithm. The fundamental frequency of the signal spectrum is indicated by the peak amplitude, as illustrated in Figure 6.

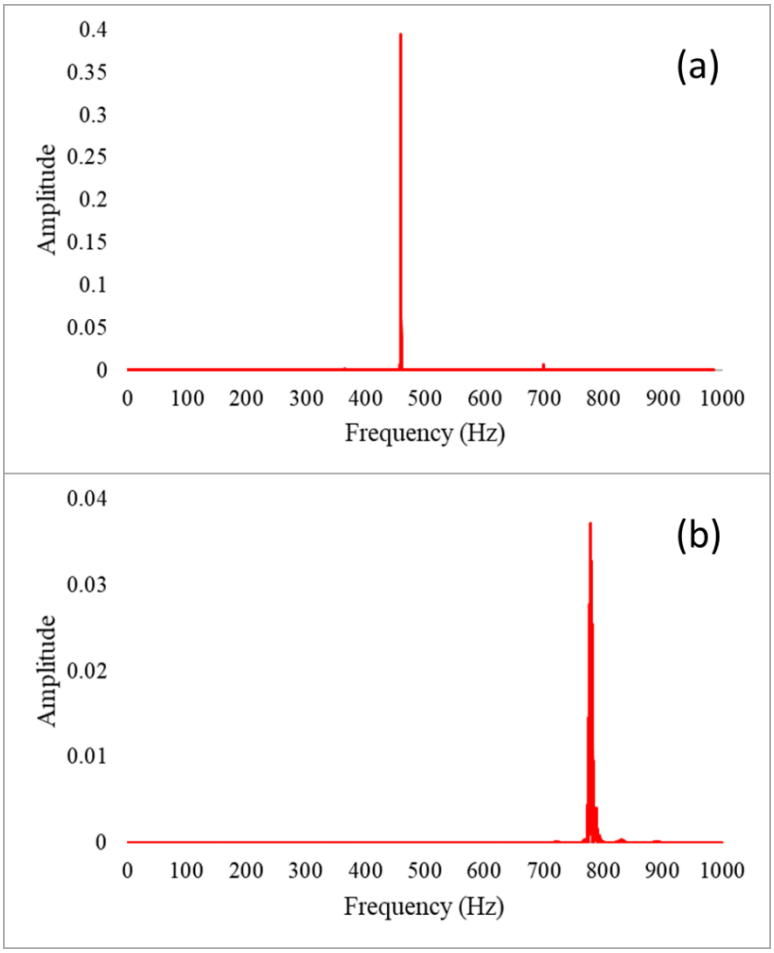

Figure 6. Power spectrum of: (a) Aluminum; (b) 3DFML specimens with 1% GNP-reinforced core and interfaces.

To calculate the damping coefficient, the signals were first filtered in LabVIEW with a bandpass of ±30 Hz to mitigate noise. Then the filtered signal envelope was retrieved using the Hilbert transform through the procedure described by Cheraghi et al. [27], using the following mathematical operation:

$$H(t) = \frac{1}{\pi}\int_{-\infty}^{+\infty} u(\tau)\frac{\chi(\tau)}{t-\tau}d\tau \quad (8)$$

where $H(t)$ is the Hilbert transform of the function $u(t)$. In practice, if the envelope being considered has a complex number, its real part includes the signal amplitude and the imaginary part contains the Hilbert operator (as it has been explained and implemented in LabVIEW by Yang et al. [63]). Finally, the averaged damping coefficient was calculated based on the logarithmic decrement of 50 successive oscillatory points of the signal within the envelope. Since the damping coefficient of aluminum is significantly smaller than that of 3DFML, the logarithmic decrement of the signals within two different periods were used in calculating the damping coefficient. In other words, the signal within a 3-second window was considered for the aluminum specimens while the signals within a window of 0.1 seconds was considered for the other specimen types.

5.4 Bending Rigidity

The specimen bending rigidity was calculated based on the experimental data and compared to analytical results. Equation (9) relates the displacement of a simply-supported 4-point bending specimen to the applied load [64].

$$\delta_{\max} = \frac{Pa}{24EI}(3L_S^2 - 4a^2) \tag{9}$$

where P is one-half of the actual total load applied to the specimen; L_S is the span length; and a is the distance between the load P and the nearest support.

Substituting for $EI = D_{11}b$ (for the composite specimens), and $a = L/3$ in Eq.(9), and solving for D_{11}, we obtain Eq.(10).

$$D_{11} = \frac{23}{1296}\left(\frac{L^3}{b}\right)\alpha \tag{10}$$

where α is P/δ, or the slope of load-displacement curve.

On the other hand, one can also calculate the analytical value of the flexural modulus of the face-sheets based on bending rigidity (per unit width) employing the mechanics of material-based expression in Eq.(11) [10]:

$$D_{11} = \frac{E_f t_f^3}{6} + \frac{E_f t_f d^2}{2} + \frac{E_c t_c^3}{12} \quad (11)$$

where t_f, t_c, E_f and E_c are the thicknesses and flexural modulus of the face-sheets and core, respectively, and d is the distance between the centroid of the face sheets (i.e., $d = t_f + t_c$).

Substituting Eq.(10) into Eq.(11) and solving for E_f yields the flexural modulus of the face sheets as per Eq.(12). The detail of testing method to identify α has been explained in 3.2.3. In this Eq., the value of E_c has been obtained from [57].

$$E_f = \frac{\frac{23}{1296}\frac{L^3}{b}\alpha - \frac{E_c t_c^3}{12}}{\frac{t_f^3}{6} + \frac{t_f (t_f + t_c)^2}{2}} \quad (12)$$

6 Results and Discussion

The results of the experiments and related analyses are presented in the present section. It should be noted that at least nine vibration tests were conducted on each specimen; therefore, the presented results for each group of specimens are the average of at least 27 tests (test were performed at least in triplicate per specimen group).

6.1 Bending Rigidities

The results of the bending rigidity were used as a parameter to normalize the main results of this investigation, i.e., frequency and damping ratio values. The values obtained from the experimental load-deflection data, and theoretically calculated values, are illustrated in Figure 7.

It should be noted that Eq.(11), which was used to give analytical solutions for the flexural modulus, is based on a formulation that homogenizes the face sheets and core constituents of the 3DFGF, yet, both the face sheets and core are inhomogeneous materials. In fact, in preform 3DFGFs the fibers (or pillars) in the core region of the 3DFGF that attach the two biaxial facial fabrics (on either side) have varying distribution in the two orthogonal directions. This degree of inhomogeneity increases in case of resin impregnated 3DFGFs reinforced with or without NCP, especially when only one of the core or face sheets are NCP reinforced. Moreover, the equation does not consider the presence of any voids or non-uniformity in resin distributions and potential

resin-rich pockets. Therefore, the simplifying assumptions used in developing the analytical solution affect the calculated value of the flexural rigidity of the complex hybrid composites considered in this study and are seen to be the cause for discrepancies noted in Figure 7. Moreover, the approach described above is based on Euler-Bernoulli theory and does not account for potential shear deformation. In general, short span sandwich beams may experience shear deformation depending on the span to depth ratio and also the degree of orthotropy of the overall beam material. Therefore, when ignoring shear deformation, relatively large discrepancies were produced when calculating the bending rigidity of the thicker beams via Eq.(11). To rectify this issue, Eq.(13) may be employed, which accounts for shear effects, to obtain values for D_{11} [47].

$$D_{11} = \frac{0.2083\alpha L^3 Gh}{10\mathrm{G}bh - 3\alpha L} \tag{13}$$

where h is the total thickness of the specimen; and G is the shear modulus of the thick 3DFGF or thick 3DFML beam calculated based on G_{P} and G_{C}, i.e., the shear moduli of the pillars and core, respectively, with the values provided in [57].

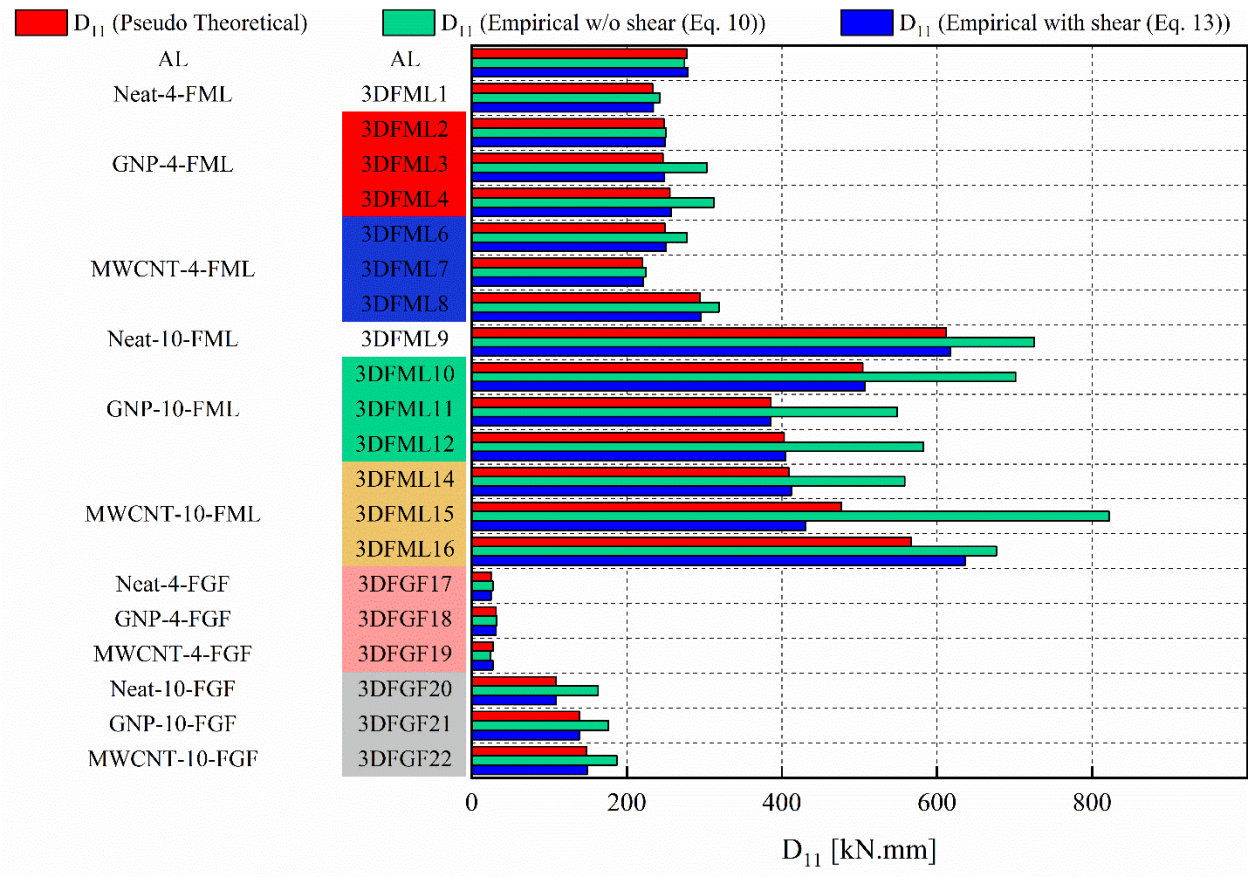

Figure 7. Specimen flexural bending rigidity obtained theoretically and experimentally via Eqs. (2), (10) and (13).

Values of D_{11} (Pseudo Theoretical) were obtained through back substituting the experimental values of frequencies, directly obtained using GS, into Eq. (2). However, both D_{11} (Empirical w/o shear (Eq. 10)), and D_{11} (Empirical with shear (Eq. 13)) were obtained based on experimental values of α which is P/δ (the slope of load-displacement curve) obtained through 4-point bending tests.

As stated earlier, sandwich specimens were also constructed for the purpose of establishing the flexural elastic modulus of the biaxial face sheets of the 3DFGF in their original (neat) form and when the fabric is reinforced with GNP and MWCNT. The values of the evaluated modulus of elasticity are reported in Table 3. This information is required for conducting further analyses, and

for comparison of experimentally obtained bending rigidity values with analytically calculated data, i.e., using Eq.(13).

Table 3. Modulus of elasticity of baseline aluminum material and 3DFGF facial fabrics with and without NCP reinforcement.

Material	E_f **(GPa)**
Al	70.00 ± 0.00
Neat fabric	9.32 ± 1.07
GNP-reinforced fabric	12.93 ± 3.38
MWCNT-reinforced fabric	18.05 ± 6.16

6.2 Fundamental Frequencies

The results of the experimentally measured frequencies by GS and LDV are tabulated in Table 4, along with values calculated using the analytical approach. The analytical results are in good agreement with the experimental data. In addition, normalized results are depicted in Figure 8. To provide a better perspective of the relative and unbiased performance of the materials, data were normalized in the following manner. Results were first divided by their respective bending rigidity, and then normalized with respect to the value for the 3DFML with neat resin (non-reinforced) and 4 mm thickness. Moreover, due to the good correlation amongst the frequency results seen in Table 4, only normalized frequency results obtained by GS are included in Figure 8 for clarity.

The normalized fundamental frequency of 3DFMLs shown in Figure 8 is lower than that of 3DFGFs, because in the case of 3DFML its 3DFGF component has been sandwiched and bonded between two thin sheets of magnesium. The data further indicates that the influence of NCP reinforcement on the fundamental frequencies, *f*, is marginal in 3DFML specimens. In few cases, the inclusion of NCP slightly affected the fundamental frequencies negatively, i.e., *f* values were slightly reduced in case of MSCNT inclusion. This can be attributed to agglomeration of NPs as it is shown in Figure 10 (b). To further examine the influence of NCP reinforcement in 3DFML specimens, resultant fundamental frequencies are presented as a function of the constituent(s) that was/were reinforced, and compared to the frequency of aluminum, as illustrated in Figure 9. The results in this figure indicate that the NCP reinforcement affected the fundamental frequency of

specimens marginally or even detrimentally, with the exception of 3DFML specimens with 10 mm thickness.

At this juncture, it is of interest to consider the morphology of NCP reinforced polymer phases, with the objective of exploring the effects that NCP addition had on the observed material responses. The examinations of samples using FESEM clearly confirmed the presence of dispersed NCP but also evidenced the existence of particle agglomerations and/or voids, as illustrated by the images shown in Figure 10. One of the reasons that NCP inclusion affects the vibration characteristics can be attributed to energy dissipation property of NCPs.

Table 4. Fundamental frequencies obtained experimentally (via GS and LDV) and analytically.

Specimen ID	f_{GS} **(Hz)**	f_{LDV} **(Hz)**	$F_{Empirical.-SF}$ **(Hz)**
Al	460.66	460.00	463.75
3DFML1	711.11	705.55	698.73
3DFML2	716.44	716.66	714.47
3DFML3	758.66	751.11	685.95
3DFML4	787.77	785.55	714.27
3DFML6	714.66	713.88	677.99
3DFML7	677.66	676.66	671.71
3DFML8	755.44	752.22	726.35
3DFML9	1067.77	1065.55	984.63
3DFML10	1050.00	1045.55	895.67
3DFML11	933.77	946.66	783.64
3DFML12	972.11	947.55	812.96
3DFML14	923.77	922.22	802.45
3DFML15	1046.44	1052.22	758.07
3DFML16	1054.11	1056.66	1017.7
3DFGF17	355.66	363.33	340.86
3DFGF18	405.11	406.66	402.21
3DFGF19	344.44	345.00	367.63
3DFGF20	683.11	682.22	559
3DFGF21	695.44	690.00	617.17
3DFGF22	674.44	673.33	602.01

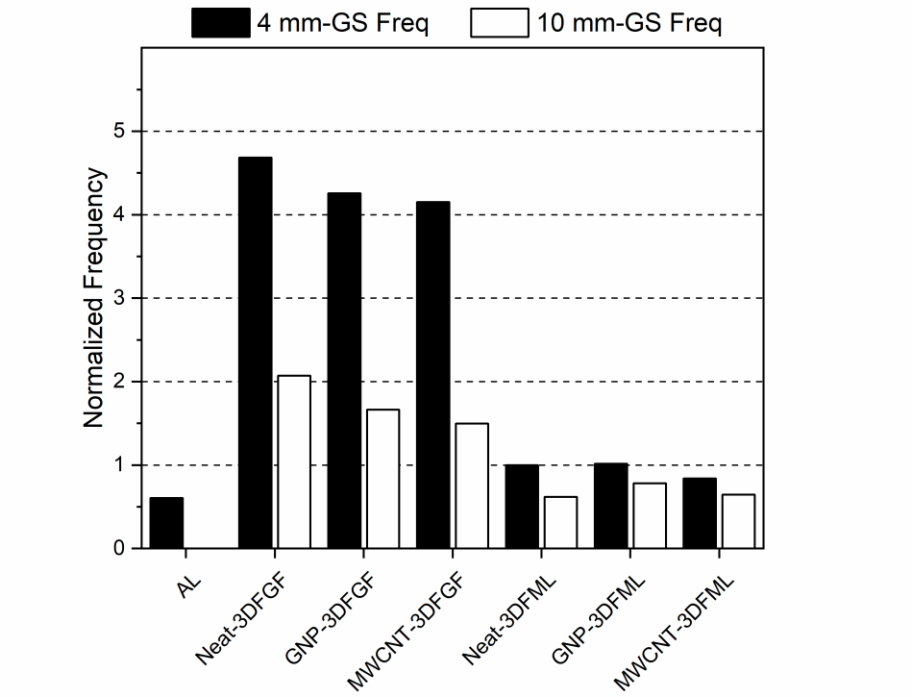

Figure 8. Influence of NCP reinforcement on fundamental frequencies of 3DFGF and 3DFML.

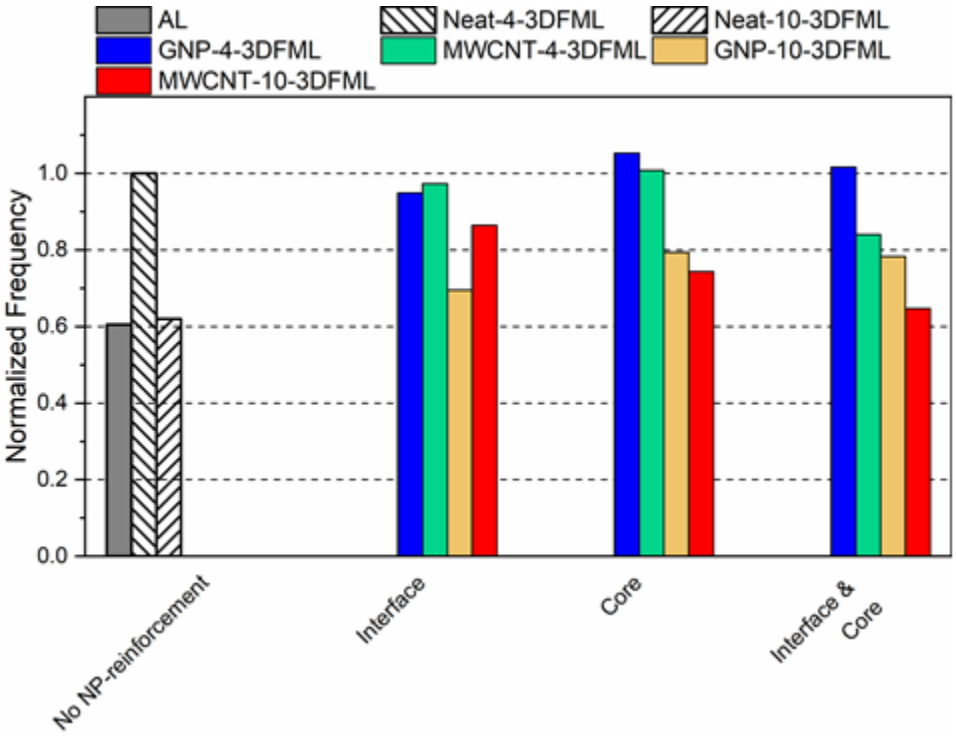

Figure 9. Influence of NCP reinforcment on the fundamental frequencies of 3DFMLs as a function reinforced constituent(s).

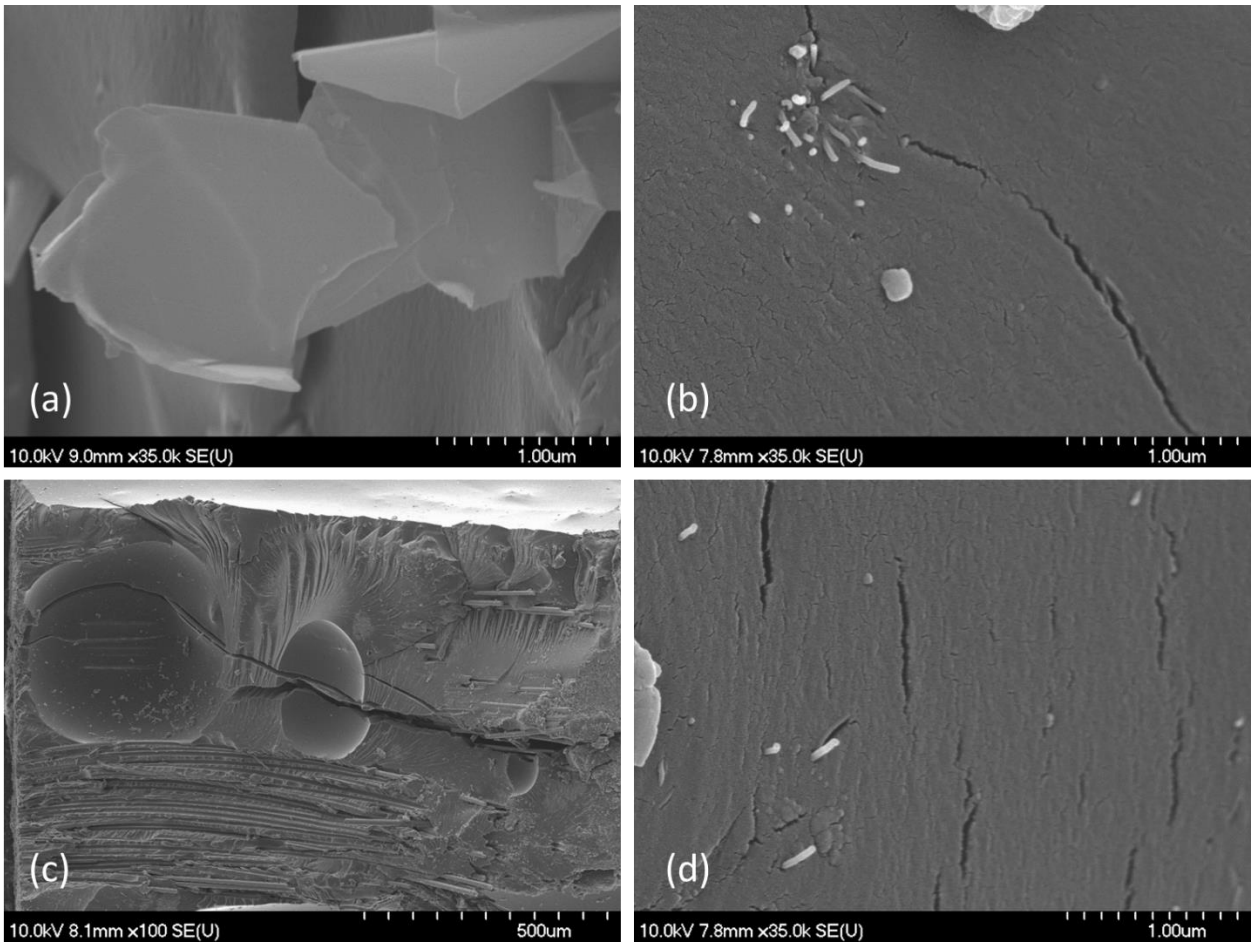

Figure 10. FESEM images of NCP reinforced 3DFML resin phase: (a) GNP; (b) MWCNT agglomeration; (c) voids; and (d) well-dispersed MWCNT reinforcement.

6.3 Damping Ratio

A high damping ratio is a desirable property for sandwich panels, and as stated earlier, other researchers have reported exemplary damping characteristics for novel sandwich panel configurations, see e.g. [19,27]. Part of the present study's objectives are (a) evaluating the damping characteristic of 3DFMLs and (b) assessing whether damping can be improved by the inclusion of NPs. Damping ratios, ξ, for all the tested material configurations are tabulated in Table 5, which shows that the calculated results based on GS and LDV measurements agree quite closely.

Table 5. Comparison of damping ratios obtained from GS and LDV measurements.

Specimen ID	ξ_{GS}	ξ_{LDV}
Al	4.79E-04	4.98E-04
3DFML1	7.17E-04	7.38E-04
3DFML2	3.42E-03	3.45E-03
3DFML3	4.01E-03	3.82E-03
3DFML4	2.42E-03	2.35E-03
3DFML6	2.62E-03	2.55E-03
3DFML7	1.68E-03	1.70E-03
3DFML8	2.54E-03	2.57E-03
3DFML9	2.15E-03	2.29E-03
3DFML10	2.31E-03	2.32E-03
3DFML11	2.84E-03	2.83E-03
3DFML12	2.30E-03	2.35E-03
3DFML14	1.92E-03	1.98E-03
3DFML15	2.24E-03	2.26E-03
3DFML16	1.86E-03	1.85E-03
3DFGF17	5.78E-03	5.67E-03
3DFGF18	6.57E-03	6.66E-03
3DFGF19	6.89E-03	6.96E-03
3DFGF20	4.14E-03	4.26E-03
3DFGF21	4.29E-03	4.43E-03
3DFGF22	4.89E-03	4.85E-03

Damping ratios were further analyzed as shown in Figure 11, which depicts data that were normalized with respect to the damping ratio of the 3DFML with neat resin (non-reinforced) and 4 mm thickness. As discussed in the previous section, NCP reinforcement did not significantly affect the fundamental frequency of 3DFML specimens. However, a significant influence of NCP reinforcement on damping ratios was observed in certain sandwich specimens. In general, damping ratios are much higher for 3DFGFs than for 3DFMLs, which can be attributed to an inherently lower damping capacity in metal-faced sandwich specimens. NCP modified resins affect the damping characteristics of GNP reinforced 3DFGFs but no clear trend can be ascertained as shown in Figure 11(a), that is, GNP seems to reduce the damping capacity of 3DFGFs while MWCNT have only a minor influence on damping capacity of 3DFGFs. Among the 3DFMLs, GNP

reinforcement yields remarkable results for the 4 mm panels as shown in Figure 11(b). When reinforcing the interface with GNP an impressive increase in the damping ratio by 234 % was determined. Improvements were even higher when the resin phase in both the interface and core was modified with GNP. However, from fabrication and cost perspective, the additional increase in damping ratio afforded by the NCP modification of the 3DFML core must be weighed against the significant effort required for processing a NCP modified resin and applying it to the core. Conversely, the use of a modified resin for bonding at the 3DFML interface is rather straightforward proposition.

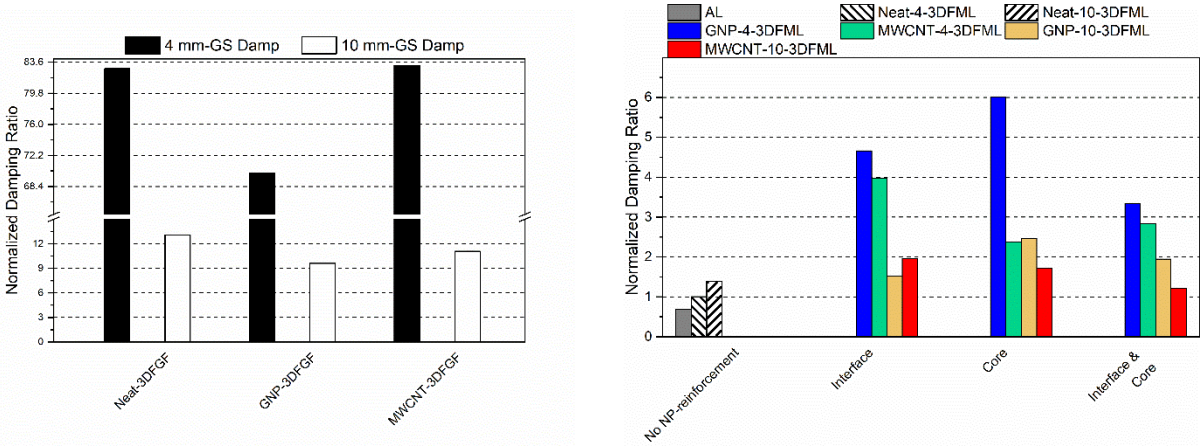

(a) (b)

Figure 11. Influence of NC-reinforcement on the damping ratio of (a) 3DFGF and (b) 3DFML hybrid materials

7 Conclusions

In the study, the vibration characteristics of 3DFGF and 3DFMLs were experimentally investigated. In addition, the effects of modifying the resin phase with GNP and MWCNT in the 3DFML and at the interface in 3DFMLs were explored. It was observed that the employed measurement systems, i.e., a Grindosonic and a laser-Doppler vibrometer device, produced repeatable results that were in good agreement. The experiments revealed that the inclusion of nanoparticles did not have an appreciable influence on increasing the fundamental frequencies of the hybrid material systems. However, nanofiller addition greatly augmented the damping ratio of certain sample types. In fact, a 1 wt% inclusion of GNP in the interface of 4 mm thick 3DFMLs

led to a significant gain of 234% in the damping ratio of the hybrid system. It was also observed that in all cases, normalized fundamental frequency and normalized damping ratio of 3DFGFs were higher than for 3DFMLs. Moreover, specimens with 4 mm core thickness exhibited a comparative higher fundamental frequency and normalized damping ratio compared to specimens with 10 mm core thickness. It should be noted that the substantial gain in damping offered by nanoparticle reinforced 3D fabrics must be considered in light of their much lower bending rigidity compared 3DFMLs (being approximately 10 times lower), which limits utilizing 3DFGF for many structural applications. In light of the findings made in this study, the 3DFML with 4 mm core thickness and 1 wt% GNP modified resin for bonding at the metal-interface proves to be an attractive material system that offers the best performance and cost-effectiveness among the system considered in this study.

Acknowledgement

The authors would like to acknowledge the financial support provided by the Natural Sciences and Engineering Research Council of Canada and the Sadler Scholarship of University of Alberta's Department of Mechanical Engineering. Finally, we thank the editors and reviewers for their constructive comments and suggestions in producing the final manuscript.

REFERENCES

[1] Hoa S V. Principles of the manufacturing of composite materials. 2009.

[2] Taheri F. Advanced fiber-reinforced polymer (FRP) composites for the manufacture and rehabilitation of pipes and tanks in the oil and gas industry. Adv. Fibre-Reinforced Polym. Compos. Struct. Appl., Elsevier; 2013, p. 662–704.

[3] Abrate S. Impact on Composite Structures. Cambridge University Press; 1998.

[4] Abrate S. Impact on laminated composites: Recent advances. Appl Mech Rev 1994;47:517–44.

[5] Al-Haik M, Borujeni AY, Tehrani M. Ballistic damage of hybrid composite materials. Adv. Fibrous Compos. Mater. Ballist. Prot., Elsevier Inc.; 2016, p. 121–43.

[6] Berthelot J-M. Composite Materials : Mechanical Behavior and Structural Analysis. Netherlands: Springer; 1999.

[7] Daniel IM, Ishai O. Engineering mechanics of composite materials. 2nd ed. New York: Oxford University Press; 2006.

[8] Mallick PK. Fibre-reinforced composites materials, manufacturing and design. 3rd ed. Boca Raton, FL: CRC Press; 2007.

[9] Reddy JN. Mechanics of Laminated Composite Plates and Shells. Boca Raton, FL: CRC Press; 2004.

[10] Zenkert D. An introduction to sandwich construction. Warrington, UK: Engineering Materials Advisory Services Ltd.; 1995.

[11] Hyer MW. Stress Analysis of Fibre-Reinforced Composite Materials. Lancaster, PA: DEStech Publication Inc.; 2009.

[12] Sayyad AS, Ghugal YM. On the free vibration analysis of laminated composite and

sandwich plates: A review of recent literature with some numerical results. Compos Struct 2015;129:177–201.

[13] Noor AK. Free vibrations of multilayered composite plates. AIAA J 1973;11:1038–9.

[14] Faires V. Design of machine elements. 4th ed. New York: Macmillan; 1965.

[15] Anlas G, Göker G. Vibration analysis of skew fibre-reinforced composite laminated plates. J Sound Vib 2001;242:265–76.

[16] Adam C. Moderately large flexural vibrations of composite plates with thick layers. Int J Solids Struct 2003;40:4153–66.

[17] Hu XX, Sakiyama T, Lim CW, Xiong Y, Matsuda H, Morita C. Vibration of angle-ply laminated plates with twist by Rayleigh-Ritz procedure. Comput Methods Appl Mech Eng 2004;193:805–23.

[18] Lei ZX, Zhang LW, Liew KM. Free vibration analysis of laminated FG-CNT reinforced composite rectangular plates using the kp-Ritz method. Compos Struct 2015;127:245–59.

[19] Chen C-S, Fung C-P, Chien R-D. Nonlinear vibration of an initially stressed laminated plate according to a higher-order theory. Compos Struct 2007;77:521–32.

[20] Kant T, Swaminathan K. Analytical solutions for free vibration of laminated composite and sandwich plates based on a higher-order refined theory. Compos Struct 2001;53:73–85.

[21] Tu TM, Thach LN, Quoc TH. Finite element modeling for bending and vibration analysis of laminated and sandwich composite plates based on higher-order theory. Comput. Mater. Sci., vol. 49, Elsevier; 2010, p. S390–4.

[22] Zou GP, Naghipour M, Taheri F. A nondestructive method for evaluating natural frequency of glued-laminated beams reinforced with GRP. Nondestruct Test Eval 2003;19:53–65.

[23] Hajikhani M, Soltannia B, Oskouei AR, Ahmadi M. Monitoring of delamination in composites by use of Acoustic Emission. 3rd Cond. Monit. Fault Diagnosis Conf., 2009.

[24] Soltannia B, Mertiny P, Taheri F. Vibration Characteristics of Multi-Wall Carbon Nanotubes (MWCNT) Reinforced 3D-Fiber Metal Laminates (3D-FML). 11th Can. Conf. Compos., 2019, p. 1–8.

[25] Soltannia B, Mertiny P, Taheri F. VIBRATION CHARACTERISTICS OF THERMALLY CYCLED GRAPHENE NANOPLATELET (GNP) REINFORCED 3D-FIBER METAL LAMINATES (3D-FML). 37th Annu. Tech. Conf. Can. Mach. Vib. Assoc., 2019, p. 1–11.

[26] De Cicco D, Taheri F. Use of a Simple Non-Destructive Technique for Evaluation of the Elastic and Vibration Properties of Fiber-Reinforced and 3D Fiber-Metal Laminate Composites. Fibers 2018;6:14.

[27] Cheraghi N, Riley MJ, Taheri F. Application of Hilbert-Huang transform for evaluation of vibration characteristics of plastic pipes using piezoelectric sensors. Struct Eng Mech 2007;25:653–74.

[28] Viens MJ, Johnson JJ. Determination of Elastic Moduli of Fiber Resin Composites Using an Impulse Excitation Technique. Greenbelt, MD, USA: 1996.

[29] Braem M, Lambrechts P, Van Doren V, Vanherle G. The Impact of Composite Structure on Its Elastic Response. J Dent Res 1986;65:648–53.

[30] Berthelot J-M. Damping Analysis of Orthotropic Composites with Interleaved Viscoelastic Layers: Modeling. J Compos Mater 2006;40:1889–909.

[31] Piollet E, Fotsing ER, Ross A, Michon G. High damping and nonlinear vibration of sandwich beams with entangled cross-linked fibres as core material. Compos Part B Eng 2019;168:353–66.

[32] Fotsing ER, Sola M, Ross A, Ruiz E. Dynamic characterization of viscoelastic materials

used in composite structures. J Compos Mater 2014;48:3815–25.

[33] Fotsing ER, Leclerc C, Sola M, Ross A, Ruiz E. Mechanical properties of composite sandwich structures with core or face sheet discontinuities. Compos Part B Eng 2016;88:229–39.

[34] Sargianis JJ, Kim HI, Andres E, Suhr J. Sound and vibration damping characteristics in natural material based sandwich composites. Compos Struct 2013;96:538–44.

[35] Taheri F. Applications of nanoparticles in adhesives: Current status. In: Pizzi A, Mittal KL, editors. Handb. Adhes. Technol. 3rd ed., Boca Raton, FL: CRC Press; 2017, p. 95–141.

[36] Soltannia B, Taheri F. Static, Quasi-Static and High Loading Rate Effects on Graphene Nano-Reinforced Adhesively Bonded Single-Lap Joints. Int J Compos Mater 2013;3:181–90.

[37] Babak Soltannia. CHARACTERIZATION OF NANOCARBON-REINFORCED AND NEAT ADHESIVES IN BONDED SINGLE LAP JOINTS UNDER STATIC AND IMPACT LOADINGS. Dalhousie University, 2013.

[38] Soltannia B, Taheri F. Influence of nano-reinforcement on the mechanical behavior of adhesively bonded single-lap joints subjected to static, quasi-static, and impact loading. J Adhes Sci Technol 2014;29:424–42.

[39] Soltannia B, Haji Gholami I, Masajedian S, Mertiny P, Sameoto D, Taheri F. Parametric Study of Strain Rate Effects on Nanoparticle-Reinforced Polymer Composites. J Nanomater 2016;2016:1–9.

[40] Soltannia B, Ahmadi-Moghadam B, Taheri F. Influence of tensile impact and strain rate on the response of adhesively bonded single lap joints. 19th Int. Conf. Compos. Mater., 2013, p. 1410–7.

[41] Ahmadi-Moghadam B, Soltannia B, Taheri F. Interlaminar crack detection in graphene

nanoplatelet/CFRP composites using electric resistance change. 19th Int. Conf. Compos. Mater., 2013, p. 3597–607.

[42] Soltannia B, Duke K, Taheri F, Mertiny P. Quantification of the Effects of Strain Rate and Nano-Reinforcement on the Performance of Adhesively Bonded Single-Lap Joints. Rev Adhes Adhes 2020:19.

[43] Ahmadi-Moghadam B, Sharafimasooleh M, Shadlou S, Taheri F. Effect of functionalization of graphene nanoplatelets on the mechanical response of graphene/epoxy composites. Mater Des 2015;66:142–9.

[44] Liu A, Wang KW, Bakis CE. Effect of functionalization of single-wall carbon nanotubes (SWNTs) on the damping characteristics of SWNT-based epoxy composites via multiscale analysis. Compos Part A Appl Sci Manuf 2011;42:1748–55.

[45] DeValve C, Pitchumani R. Experimental investigation of the damping enhancement in fiber-reinforced composites with carbon nanotubes. Carbon N Y 2013;63:71–83.

[46] Khan SU, Li CY, Siddiqui NA, Kim J-K. Vibration damping characteristics of carbon fiber-reinforced composites containing multi-walled carbon nanotubes. Compos Sci Technol 2011;71:1486–94.

[47] Chamis CC. Analysis of the three-point-bend test for materials with unequal tension and compression properties. Cleveland, Ohio: 1974.

[48] ASTM E756 - Standard Test Method for Measuring Vibration-Damping Properties of Materials. Philadelphia, USA: 2017.

[49] ASTM D3039 - Standard Test Method for Tensile Properties of Polymer Matrix Composite Materials. Philadelphia, USA: 2017.

[50] GrindoSonic: The Impulse Excitation Technique with Applications for Composites and Plastics n.d. http://www.grindosonic.com/applications/composites_plastics.html.

[51] Wisnom MR. Mechanisms to create high performance pseudo-ductile composites. IOP Conf. Ser. Mater. Sci. Eng., vol. 139, Institute of Physics Publishing; 2016.

[52] Asundi A, Choi AYN. Fiber Metal Laminates: An Advanced Material for Future Aircraft. J Mater Process Technol 1997;63:384–94.

[53] Vermeeren CAJR. An Historic Overview of the Development of Fibre Metal Laminates. Appl Compos Mater 2003;10:189–205.

[54] Vlot A. Glare history of the development of a new aircraft material. Kluwer Academic Publishers; 2004.

[55] Marissen R. Fatigue crack growth in ARALL: A hybrid aluminium-aramid composite material: Crack growth mechanisms and quantitative predictions of the crack growth rates. Delft University of Technology, 1988.

[56] Asaee Z, Taheri F. Experimental and numerical investigation into the influence of stacking sequence on the low-velocity impact response of new 3D FMLs. Compos Struct 2016;140:136–46.

[57] De Cicco D, Taheri F. Robust numerical approaches for simulating the buckling response of 3D fiber-metal laminates under axial impact – Validation with experimental results. J Sandw Struct Mater 2018:1–30.

[58] China Beihai Fiberglass Co. Ltd. n.d. http://www.fiberglassfiber.com/Item/Show.asp?m=5&d=345 (accessed January 16, 2020).

[59] ASTM D7249 - Standard Test Method for Facesheet Properties of Sandwich Constructions by Long Beam Flexure. Philadelphia, USA: 2018.

[60] Tedesco JW, McDougal WG, Allen Ross C. Structural dynamics : theory and applications. Menlo Park, CA: Addison Wesley Longman; 1999.

[61] Kelly SG. Fundamentals Of Mechanical Vibration. 2nd ed. New York: McGraw-Hill Education; 1992.

[62] Naghipour M, Mehrzadi M, Taheri F, Zou GP. Polynomial correction function for half-power bandwidth (HPB) method of damping of glulam beams reinforced with E-glass reinforced epoxy polymer (GRP). Can J Civ Eng 2009;36:241–52.

[63] Yang X, Ji S, Song L. Signal Analysis and Processing Platform Based on LabVIEW. Sensors & Transducers 2014;172:165–71.

[64] Gere JM. Mechanics of Materials. Sixth. Belmont, CA: Brooks/Cole –Thomson Learning; 2004.